Conversion of jet biofuel range hydrocarbons from palm oil over zeolite hybrid catalyst

Norsahika Mohd Basir[1] , Norkhalizatul Akmal Mohd Jamil[2] and Halimaton Hamdan[1,2]

Abstract

The catalytic conversion of palm oil was carried out over four zeolite catalysts—Y, ZSM-5, Y-ZSM-5 hybrid, and Y/ZSM-5 composite—to produce jet biofuel with high amount of alkanes and low amount of aromatic hydrocarbons. The zeolite Y-ZSM-5 hybrid catalyst was synthesized using crystalline zeolite Y as the seed for the growth of zeolite ZSM-5. Synthesized zeolite catalysts were characterized by X-ray diffraction, Fourier transform infrared spectroscopy, field-emission scanning electron microscopy, and temperature programmed desorption of ammonia, while the chemical compositions of the jet biofuel were analyzed by gas chromatography-mass spectrometry (GC-MS). The conversion of palm oil over zeolite Y resulted in the highest yield (42 wt%) of jet biofuel: a high selectivity of jet range alkanes (51%) and a low selectivity of jet range aromatic hydrocarbons (25%). Zeolite Y-ZSM-5 hybrid catalyst produced a decreased percentage of jet range alkane (30%) and a significant increase in the selectivity of aromatic hydrocarbons (57%). The highest conversion of palm oil to hydrocarbon compounds was achieved by zeolite Y-ZSM-5 hybrid catalyst (99%), followed by zeolite Y/ZSM-5 composite (96%), zeolite Y (91%), and zeolite ZSM-5 (74%). The reaction routes for converting palm oil to jet biofuel involve deoxygenation of fatty acids into C15–C18 alkanes via decarboxylation and decarbonylation, catalytic cracking into C8–C14 alkanes, and cycloalkanes as well as aromatization into aromatic hydrocarbon.

Keywords

Jet biofuel, palm oil, fatty acids, zeolite, zeolite Y-ZSM-5 hybrid catalyst

Introduction

Global primary energy consumption increases by 37% between 2013 and 2035. Fossil fuels remain the dominant form of energy in 2035 with a share of 81%, down from 86% in 2013.[1,2] The development of renewable fuel resources has attracted considerable attention because of the global environmental concerns and the exhaustion of the fossil fuel resources.[3] A viable alternative way of solving these problems is the production of hydrocarbon from inexpensive biomass waste sources. The current share of biomass in the net final energy consumption by end-use sector is 14%, which comprises heating and cooling at 12.6%, transportation at 0.8%, and electricity at 0.4%.[4] The

increasing demand by the aviation industry for alternative fuels that offers potential environmental benefits has accelerated advances in exploring new generation of renewable

[1] Department of Chemistry, Faculty of Science, Universiti Teknologi Malaysia, Johor, Malaysia
[2] Razak Faculty of Technology and Informatics, University Teknologi Malaysia, Jalan Sultan Yahya Petra, Kuala Lumpur, Malaysia

Corresponding author:
Halimaton Hamdan, Razak Faculty of Technology and Informatics, Universiti Teknologi Malaysia, Jalan Sultan Yahya Petra, 54100 Kuala Lumpur, Malaysia.
Email: halimatonhamdan@utm.my

biofuel sources. Biomass, also known as lignocellulosic material, represents a valid alternative source to initially produce liquid bio-oil and finally jet biofuel, without competing with food crops, and promote the reduction of carbon emission.[5] Bio-oil derived from the pyrolysis of biomass is considered to be a promising second-generation energy-laden fuel.

Jet fuel from petroleum refining, a type of aviation fuel, has a growing market demand because of the rapid development in the aircraft industry.[6] Consequently, the increase of petroleum oil prices, environmental concerns, and uncertainties of petroleum availability spur interest in exploring the potential of biomass-derived jet fuels (jet biofuel) as an alternative to fossil fuel. Liquid jet biofuel derived from plant oil, such as sunflower oil, soybean oil, palm oil, rapeseed oil, and algae oil, has been extensively studied by many researchers.[7–10] The production of jet fuels is required to follow highly stringent international standards, which makes it more difficult to develop alternative fuel using biomass resources. Currently, researchers propose several methods to convert biomass materials to biojet fuel, which include hydroprocessing, pyrolysis, Fischer–Tropsch gasification, or advanced gas fermentation process.[11–13] Among these methods, catalytic fast pyrolysis is recognized as the most established and efficient single process. Fast pyrolysis performs thermochemical decomposition of lignocellulosic compound through rapid heating at a temperature range of 350–800°C in the absence of oxygen, converting it to liquid bio-oil with gas and char as byproducts.[14–16]

The major producers of palm oil in Southeast Asia are Indonesia and Malaysia. The intense research, developmental, and commercial activities of the palm oil industry in these countries have led to immense interest in developing green aviation biojet fuel from renewable biomass materials. Li et al.[9] investigated jet biofuel production from palm oil using mesoporous zeolite catalysts impregnated with nickel (Ni) and has successfully converted it into 53% of jet range alkane and 17% of jet range aromatics. Oil palm biomass has outstanding properties and may be converted into jet biofuel due to the presence of a considerable amount of fatty acids (C16–C18) and relatively low oxygen content that can be easily removed by deoxygenation process. To meet the international specifications of low jet range alkane, the biojet fuel from palm oil that contains high amount of fatty acids can be processed through several routes, which are catalytic deoxygenation reactions, including decarboxylation or decarbonylation and carbon chain cracking.[17]

Various heterogeneous catalysts have been tested for the conversion of fatty acids in palm oil wherein the choice of catalysts is vital especially during catalytic cracking process. Zeolites have been efficiently applied in the petrochemical industry as molecular sieves, adsorbents, and heterogeneous catalyst due to the framework nanostructure, ion-exchange abilities, chemical composition, pore size distribution, and both acidic–basic characteristics.[18–20] For example, zeolite A may have been efficiently applied in the petrochemical industry as molecular sieves and adsorbent, whereas zeolite Y has been applied as heterogeneous catalyst for cracking and hydrocracking of hydrocarbon molecules into oil and gas. However, the pore size of zeolite Y needs further modification to improve the cracking efficiency of heavy hydrocarbon bio-oil to light jet range alkane.

Zeolite Y is the main active catalyst of the catalytic cracking process because of its strong acidity, high porosity, and hydrothermally stable properties.[20] Nevertheless, the pore size of zeolite Y (0.74 nm × 0.22 nm) prevents the cracking of larger molecules that occur on the external surface structure of zeolite Y. To improve the cracking activity of heavy hydrocarbon to light jet range alkane, an additive component needs to be added to zeolite Y catalyst. Zeolite ZSM-5 has been used as an additive component to increase gasoline octane number and light olefins.[21] Since zeolite Y and ZSM-5 are highly active in catalytic cracking, the combination of these two zeolites can be applied to improve jet range alkane, hence reducing the formation of aromatic hydrocarbons.

In the present work, hybrid zeolite nanocatalyst composed of zeolite Y and ZSM-5 is synthesized by employing zeolite Y as nutrients for the growth of ZSM-5. The conversion of palm oil directly to jet biofuel range alkane and aromatic hydrocarbons over zeolites Y, ZSM-5, Y-ZSM-5 hybrid, and Y/ZSM-5 composite by pyrolysis process is tested and analyzed. The reaction pathways to produce jet biofuel range alkane and aromatic hydrocarbons are proposed.

Experimental details

Materials

Rice husk ash (RHA, 95 wt% SiO_2) was obtained from the Zeolite and Nanostructured Materials Laboratory, UTM, Malaysia.[22] Aluminum oxide anhydrous (Al_2O_3, Bendosen, CCM Chemicals Malaysia), sodium aluminate anhydrous (NaAlO$_2$, Riedel-de Haen, Germany), sodium hydroxide (NaOH, Merck, USA), sulfuric acid (H_2SO_4, Merck, USA), and tetrapropylammonium bromide (TPABr, Sigma-Aldrich, USA) were directly used without purification. The palm oil used in the experiments was purchased from the local market. Distilled water was used in the synthesis, preparation of the solution, and purification of the solid samples.

Synthesis of zeolite Y

The synthesis of zeolite Y was prepared using hydrothermal method reported by Hamdan and Keat.[23] Zeolite Y was synthesized according to the molar composition of $6.4Na_2O:1Al_2O_3:12SiO_2:180H_2O$ via direct synthesis.

NaOH solution was prepared by dissolving 21.64 g of NaOH pellets in 200 mL of distilled water under stirring. Aluminate solution was prepared by the dissolution of $NaAlO_2$ (19.56 g) and NaOH solution (50 mL) in a Teflon bottle under vigorous stirring and heated until the mixture became clear. In a separate Teflon bottle, 47.97 g of RHA was mixed with 150 mL of the prepared NaOH solution and heated at 95°C for 2 h with stirring. The aluminate solution was then added slowly to the silicate solution and the mixture was left at room temperature to homogenize for 2 h under continuous stirring. Next, the Teflon bottle was tightly sealed and aged for 8 h at 105°C in the oven. The obtained solid product was separated from the aqueous phase by filtration and washed until the pH of the filtrate was below 10, followed by drying in the oven at 100°C for 24 h. Finally, the as-synthesized zeolite Y was calcined at 550°C for 550 min.

Synthesis of zeolite ZSM-5

In a typical synthesis, 0.30 g of Al_2O_3 was mixed with 0.11 g of NaOH and 10 mL of distilled water and was stirred at room temperature. Subsequently, another 2.95 g of NaOH and 15 mL of distilled water were added to the solution. An aqueous solution of TPABr was prepared separately by mixing 4.00 g of TPABr with 1.7 mL of concentrated H_2SO_4 and 50 mL of distilled water. In the next step, 9.00 g of RHA was predispersed in 21 mL of distilled water under stirring. The prepared aluminate and TPABr solutions were then added simultaneously to the silica solution in a Teflon bottle and homogenized with continuous stirring for 30 min. The pH of the gel must be between 11 and 12 before the crystallization process. Next, the gel was transferred into a Teflon bottle, tightly sealed, and aged in an oven at 96°C for 7 days. The white solid formed was filtered, washed with plenty of distilled water until pH 8, and dried in an oven at 100°C for 24 h. The white powder of zeolite ZSM-5 was then calcined at 550°C for 4 h and maintained for 5 h.

Synthesis of zeolite Y-ZSM-5 hybrid

Zeolite Y-ZSM-5 hybrid was prepared based on other published works with modified compositions and types of raw materials[21]. The zeolite hybrid material was synthesized by hydrothermal method, which produced highly crystalline product without further heat treatment. Typically, 0.60 g of NaOH, 2.00 g of TPABr, 3.94 g of RHA, and 9.00 g of as-synthesized zeolite Y were added to 100 mL distilled water. The mixture was stirred for 1 h at room temperature, then transferred into a Teflon-lined stainless-steel autoclave, and crystallized at 180°C in static condition for 22 h. The solid product was filtered, washed with distilled water until pH 9, and dried at 100°C for 24 h. Finally, the product was calcined at 550°C for 6 h and labeled as Y-ZSM-5 hybrid.

Synthesis of zeolite Y/ZSM-5 composite

Zeolite Y/ZSM-5 composite was prepared by physical mixing of zeolite Y and ZSM-5 with a mass ratio of 1:1. Typically, 2.50 g of zeolite Y was mixed with 2.50 g of zeolite ZSM-5 and stirred for 2 h at room temperature. The mixture was milled in a mortar and then calcined at 550°C for 6 h.

Modification of zeolite by ion exchange

The zeolite Y, ZSM-5, Y-ZSM-5 hybrid, and Y/ZSM-5 composite were ion exchanged with NH^{4+} cations to protonate zeolite to create Brönsted acidity. In a typical preparation, 1 g of as-synthesized Na^+-zeolite samples was added to 50 mL of 1M NH_4NO_3 aqueous solution and stirred for 2 h at 60°C. The suspended NH^{4+}-zeolite solid was filtered, washed with distilled water, and air dried. The H^+-zeolite was obtained by calcination at 500°C for 3 h.

Preparation of jet biofuel

The palm oil conversion experiment was carried out in a 500-mL batch reactor equipped with an external heating mantle. In this process, 200 mL of palm oil and catalyst with a mass ratio of 20:1 was loaded into the reactor, which was then vigorously stirred for 1 min. Thereafter, the reactor was sealed and purged with flowing hydrogen for about 20 min to set the pressure and temperature. The reaction was carried out at 390°C while stirring at 300 r min^{-1}. After the reaction, the liquid-phase products were collected and separated via centrifugation. The liquid products were analyzed using GC-MS.

Characterizations

The infrared spectra of the samples were recorded on a Perkin Elmer (USA) Fourier transform infrared (FTIR) using the KBr pellet method, with 20 s scans, in the wavenumber range of 1600–400 cm^{-1} and resolution of 4 cm^{-1}.

The powder X-ray diffraction (XRD) data were collected on a Bruker (Germany) D8 Advance X-ray diffractometer using Ni-filtered copper K_α radiation ($\lambda = 1.5418$ Å) at 45 kV and 40 mA in the range of $2\theta = 5$–$50°$ with vertical goniometer at room temperature. A step interval of $0.05° 2\theta$ with a count time of 1 s per step was used. Reflection positions and d-spacings were determined from the raw data using the automated data analysis programs.

Field-emission scanning electron microscopy (FESEM) was monitored on a JEOL (Japan) JSM-670F to determine the surface morphology of the samples. Prior to scanning, the samples were coated with platinum or carbon film using SEM auto fine-coater unit, model JEC-3000FC, or EC-32010CC, respectively.

The acidity of catalysts was determined by temperature programmed desorption of ammonia (NH_3-TPD) analysis and measured using the Micromeritics (USA) AutoChem 2920 V403 instrument. NH_3-TPD was carried out in a flow-
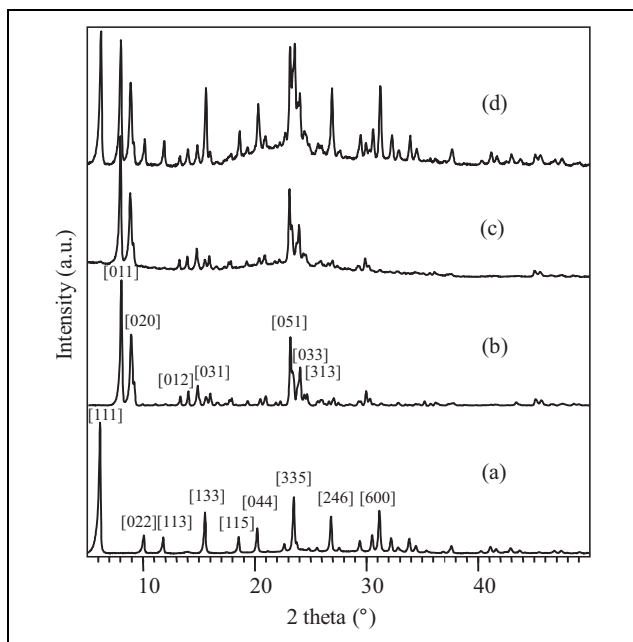
Figure 1. XRD diffractogram of zeolites (a) Y, (b) ZSM-5, (c) Y-ZSM-5 hybrid, and (d) Y/ZSM-5 composite. XRD: X-ray diffraction.

type fixed-bed reactor and loaded with 0.10 g sample at 300°C under high-purity He flow at 30 mL min^{-1} for 60 min. The sample was cooled at 20 mL min^{-1} by 10% NH$_3$-He to 120°C for 60 min. The sample was then purged with high-purity He at 30 mL min^{-1} for 1 h and heated to 700°C (10°C min^{-1}). The amount of ammonia desorbed was quantitatively analyzed by the thermal conductivity detector.

Prior to the GC analysis, the liquid-phase products were diluted in CCl$_3$ at a ratio of 1:10 and analyzed using the Agilent 6890N/5973 MSD equipped with the HP-5MS capillary column (30 m × 250 μm × 0.25 μm). The injection temperature was set at 280°C. The GC oven temperature was programmed as follows: 4-min hold at 50°C, 2°C min^{-1} ramping to 80°C, 10-min hold at 80°C, 10°C min^{-1} ramping at 300°C, and 10-min hold at 300°C. The GC-MS results were quantified using the peak area normalization method based on the peak area percentages of the identified components. The area percent of changed concentrations of palm oil compounds obtained from GC-MS results was used to predict product concentration in jet biofuel.

Results and discussion

### Physical properties of zeolite catalysts

The XRD diffractograms of zeolites Y, ZSM-5, Y-ZSM-5 hybrid, and Y/ZSM-5 composite are shown in Figure 1. For phase identification, the XRD patterns of all samples were compared with the standard patterns of faujasitic (FAU)-type zeolite Y and mobil five (MFI)-type ZSM-5 zeolites. XRD pattern of zeolite Y matches the standard XRD pattern of FAU-type zeolite (reference code: 98-016-9078).[24]

The main XRD reflections at 2θ values of 6.17°, 15.56°, 23.49°, and 27.58° are attributed to (111), (133), (335), and (246) crystal planes, respectively, ascribing to the FAU structure of crystalline zeolite Y. The X-ray diffractogram of ZSM-5 clearly shows a pattern characteristic of MFI-type zeolite framework structure (reference code: 98-015-9834).[25] The XRD pattern consists of a series of intense peaks at 2θ value ranges of 7−9° and 23−25°, corresponding to the (101), (200), (501), (303), and (133) planes, respectively. However, the characteristic reflections of synthesized zeolite ZSM-5 are less intense and broader than those of the standard reference, presumably because of its relatively lower degree of crystallinity and smaller crystallite size.[26]

It is observed that Y/ZSM-5 composite prepared by physical mixing displays the overlapping characteristic peaks of FAU and MFI structures, indicating the physical coexistence of zeolite Y and ZSM-5 phases (Figure 1(d)). The peaks at 6.27°, 10.18°, and 23.59° are the characteristic diffraction peaks of zeolite Y, while the peaks at 8.03°, 8.88°, 23.16°, and 24.05° are the characteristic diffraction peaks of ZSM-5. In contrast, the XRD pattern of zeolite Y-ZSM-5 hybrid is dominantly represented by the zeolite ZSM-5 phase with much decreased intensity of the zeolite Y phase (Figure 1(c)). This indicates that the smaller zeolite Y crystallites are embedded in the continuous zig-zag channels and on the surface of the ZSM-5 framework.[27] Therefore, it can be deduced from Figure 1(c) that in the zeolite Y-ZSM-5 hybrid, nanostructured framework of zeolite ZSM-5 exists as the main phase, in which the smaller zeolite Y crystallites are embedded and appear homogeneous to XRD. Consequently, the characteristic peaks of zeolite Y phase may completely disappear.

The morphology of zeolite Y, ZSM-5, Y-ZSM-5 hybrid, and Y/ZSM-5 composite is shown in Figure 2(a), (b), (c), and (d), respectively. The FESEM image in Figure 2(a) displays cubic zeolite Y crystals of uniform size with an average diameter of 300 nm. The morphology of zeolite ZSM-5 in Figure 2(b) shows many layers of elongated hexagonal prismatic structure with smoother and less aggregated surface. The crystalline structure is 500–600 nm in length and 100–200 nm in thickness. ZSM-5 crystals are apparently fused together forming agglomerates. Some amorphous silica particles of 10–50 nm in diameter are observed on the surface of both zeolite Y and ZSM-5.[28]

Figure 2(c) reveals the morphology of the zeolite Y-ZSM-5 hybrid. The hybrid product constitutes a compact structure of larger aggregates composed of intergrown Y-ZSM-5 zeolite particles of variable sizes. The cubic structure of zeolite Y is not well defined but some Y crystals can be observed. This observation supports the disappearance of zeolite Y phase in the XRD pattern, which may be caused by the encapsulation of zeolite Y by the bigger framework of zeolite ZSM-5 crystals during synthesis. These results are similar with those observed and reported by Pan et al.,[27] where zeolite Y crystals are swallowed by
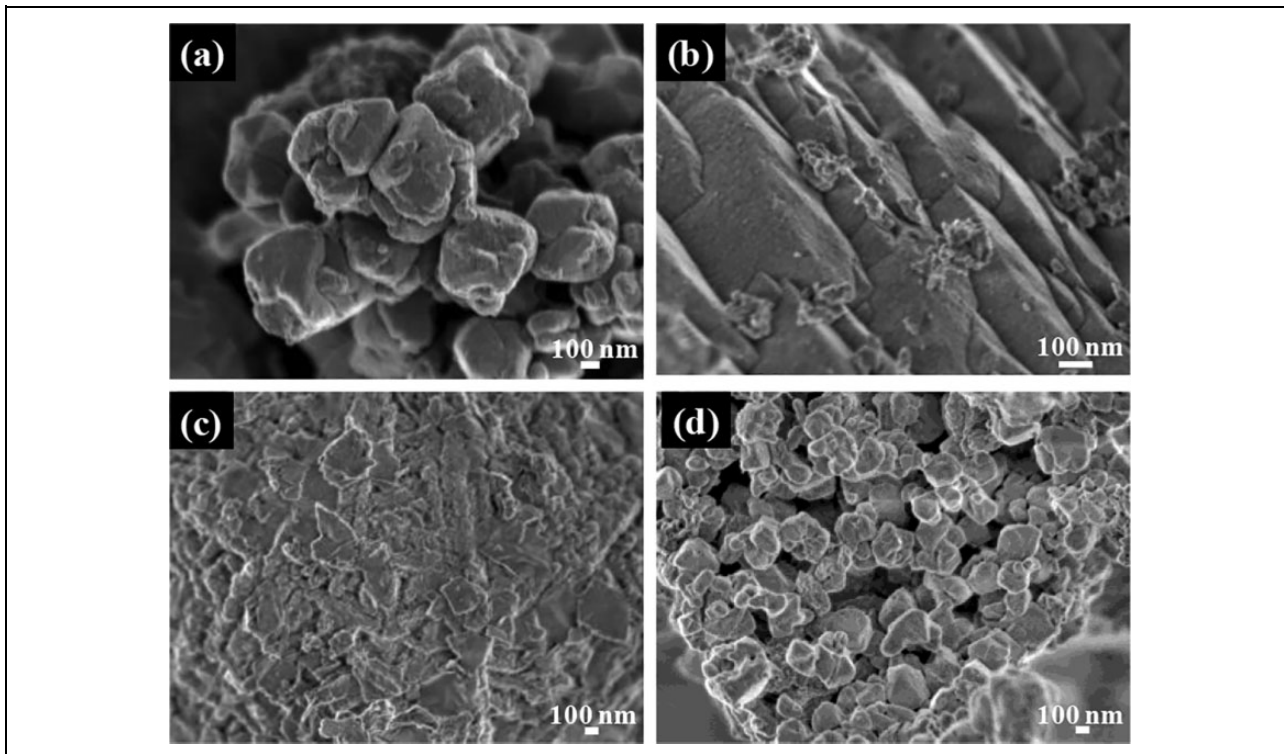
Figure 2. FESEM images of zeolites (a) Y (magnification: ×50,000), (b) ZSM-5 (magnification: ×85,000), (c) Y-ZSM-5 hybrid (magnification: ×35,000), and (d) Y/ZSM-5 composite (magnification: ×35,000). FESEM: field-emission scanning electron microscopy.

the larger ZSM-5 particles. Comparatively, the image of zeolite Y/ZSM-5 composite demonstrates the physical mixture of zeolite Y with ZSM-5 crystals (Figure 2(d)). The image shows that the bigger spherical agglomerates of zeolite ZSM-5 are entirely covered by the nanoaggregates of cubic zeolite Y structures. Evidently, the synthesis of zeolite composite by physical mixing still retains the original morphology of each zeolite.

Chemical properties of catalysts

Structural properties of zeolite Y, ZSM-5, Y-ZSM-5 hybrid, and Y/ZSM-5 composite were recorded using FTIR spectroscopy in the range of $4000-450$ cm^{-1} (Figure 3). Generally, the FTIR spectra of zeolites can be divided into two regions at $4000-3000$ cm^{-1} and $1300-450$ cm^{-1}. The spectra of zeolites in the range of $1300-400$ cm^{-1} region correspond to the framework vibrations of lattice cell (T$-$O$-$T unit), where T is SiO$_4$ or AlO$_4$ tetrahedron, while the $4000-3000$ cm^{-1} region is attributed to hydroxyl groups attached to the framework zeolite structure. All zeolite samples show a strong broad absorption band in the wavenumber region $1000-1100$ cm^{-1} assigned to the asymmetric stretching vibrations of tetrahedral SiO$_4$ and generally shift to higher wavenumbers with the increasing silica ratio of the zeolite.[29] The band at around 1640 cm^{-1} and 460 cm^{-1} is assigned to the scissor vibration arising from the proton vibration in the water molecule and TO$_4$
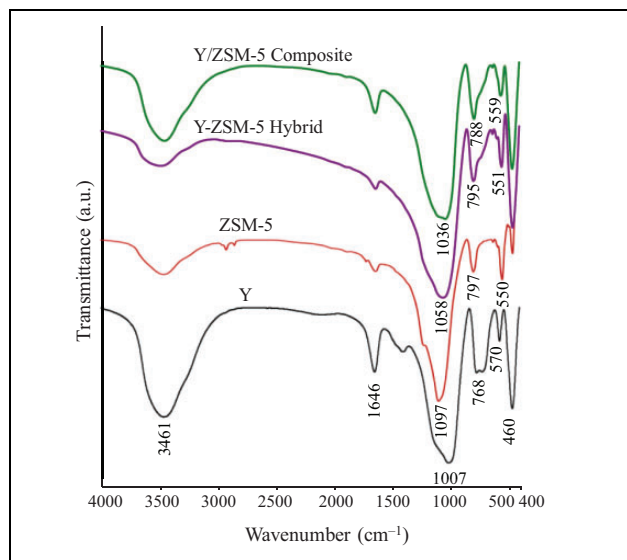

Figure 3. FTIR spectra of zeolites Y, ZSM-5, Y-ZSM-5 hybrid, and Y/ZSM-5 composite. FTIR: Fourier transform infrared.

bending vibrations of the SiO$_4$ and AlO$_4$ internal tetrahedral, respectively. The spectra demonstrate that the presence of broadband at $3456-3487$ cm^{-1} is resulted from the O$-$H stretching mode from water physisorbed on the surface of zeolites.

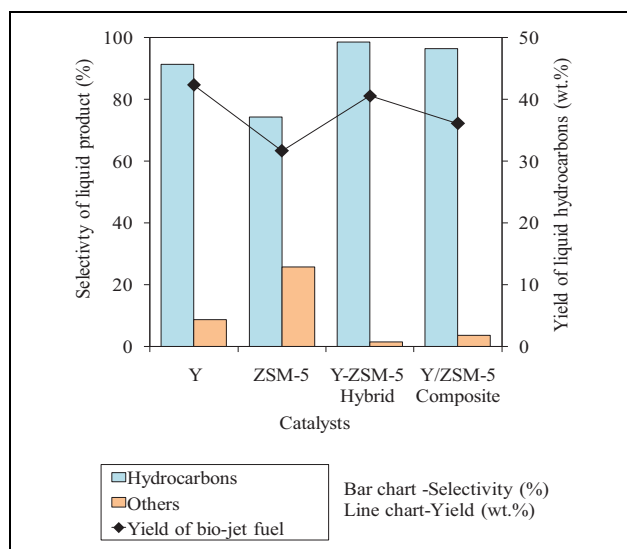FTIR spectrum of zeolite Y shows absorption band at 570 cm^{-1}, which is attributed to the double ring external
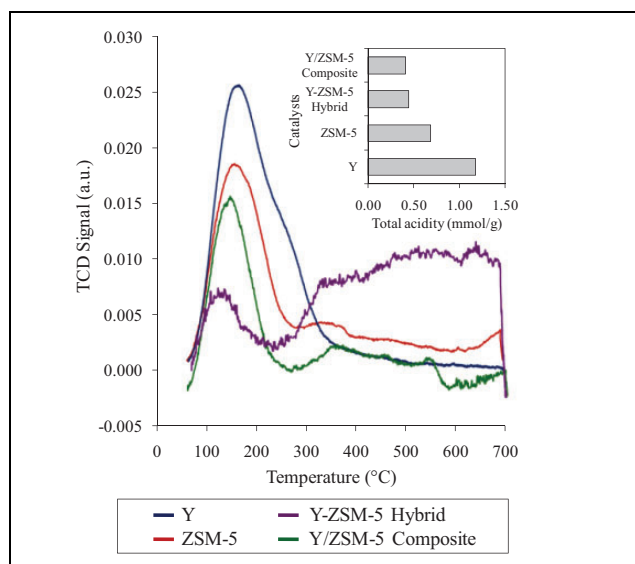
Figure 4. NH$_3$-TPD profile of zeolites Y, ZSM-5, Y-ZSM-5 hybrid, and Y/ZSM-5 composite. In the insets, total acidity (mmol NH$_3$/g) of the catalysts. NH$_3$-TPD: temperature programmed desorption of ammonia.


Figure 5. Selectivity and yield of liquid product composition converted from palm oil over zeolites Y, ZSM-5, Y-ZSM-5 hybrid, and Y/ZSM-5 composite catalyst in the batch reactor (catalyst: 10 g, palm oil: 200 mL, reaction time: 2 h, and reaction temperature: 390°C).

linkage peak associated with the FAU structure. Nevertheless, the band at 550 cm^{-1} of zeolite ZSM-5 is due to vibrations related to the double five-membered rings lattice of the external linkages, which are sensitive to the framework structure. As shown in Figure 3, zeolite Y shows a sharp medium band at 768 cm^{-1}, assigned to internal tetrahedral symmetrical stretching, while zeolite ZSM-5, Y-ZSM-5 hybrid, and Y/ZSM-5 composite show bands at higher wavenumber around 788−797 cm^{-1}, attributed to the symmetric stretching of the external linkages. Meanwhile, for the Y-ZSM-5 hybrid and Y/ZSM-5 composite, the band at 570 cm^{-1} is weakened and shifted to lower wavenumber of 551 and 559 cm^{-1}, respectively. The result suggests that the framework of zeolite Y is broken with the simultaneous formation of ZSM-5 phases, specifically for zeolite Y-ZSM-5 hybrid, as confirmed by XRD analysis.

The strength and amount of acidity of zeolite catalysts are evaluated by the NH$_3$-TPD. Figure 4 shows the NH$_3$-TPD curves and total surface acidity of the prepared zeolite catalysts. It is observed that two NH$_3$ desorption peaks are detected in the range of 150–300°C and 300–600°C, assigned to weak and strong acidity, respectively. Quantitatively, zeolite Y exhibits a maximum number of acid sites (1.177 mmol g^{-1}) higher than measured in zeolite ZSM-5 (0.683 mmol g^{-1}). However, the total acid concentration of synthesized Y-ZSM-5 hybrid and Y/ZSM-5 composite is 0.443 and 0.409 mmol g^{-1}, respectively, which are lower than the parent zeolites.

Catalytic performance

Figure 5 shows the selectivity and yield of liquid product composition after the reaction of palm oil over zeolites Y,

ZSM-5, Y-ZSM-5 hybrid, and Y/ZSM-5 composite as catalysts. Generally, the conversion of palm oil to jet biofuel was >70% for all the reactions. Liquid jet biofuel, solid carbonaceous residue (char) from thermal degradation, and noncondensable gas were the main products of the reactions. A high yield of jet biofuel (42 wt%) was obtained over zeolite Y catalyst with hydrocarbon selectivity of 91%. The high selectivity of hydrocarbon products over zeolite Y is due to the high amount of acid sites present and its pore size.[30] Comparatively, the yield of jet biofuel over zeolite ZSM-5 catalyst is 32 wt% and the selectivity for hydrocarbon is 74%. The smaller pore size of ZSM-5 (0.54 nm) as compared to the zeolite Y (0.74 nm) limits the diffusion of large molecules of palm oil fatty acid, forcing them to be cracked into shorter chain hydrocarbons at the outer surface of the catalyst. The large fatty acids were not able to diffuse in the pore and access the active sites, resulting in low conversion to hydrocarbon compounds. Evidently, the large pore size of zeolite Y enhanced diffusion of deoxygenated fatty acids in the pores and cracking into short hydrocarbon chains.

Interestingly, GC-MS analysis shows that the conversion of palm oil using zeolites Y-ZSM-5 hybrid (99%) and Y/ZSM-5 composite (96%) resulted in a remarkably enhanced production of hydrocarbon compounds. Nevertheless, the yield of liquid jet biofuel product decreased to 41 and 36 wt% over zeolite Y-ZSM-5 hybrid and Y/ZSM-5 composite, respectively, presumably to the decreasing concentration of acid sites. This indicates that the amount of acid sites plays an important role in determining the yield of liquid jet biofuel product.

FTIR spectra of palm oil and jet biofuel products are shown in Figure 6. The FTIR spectra of palm oil show a
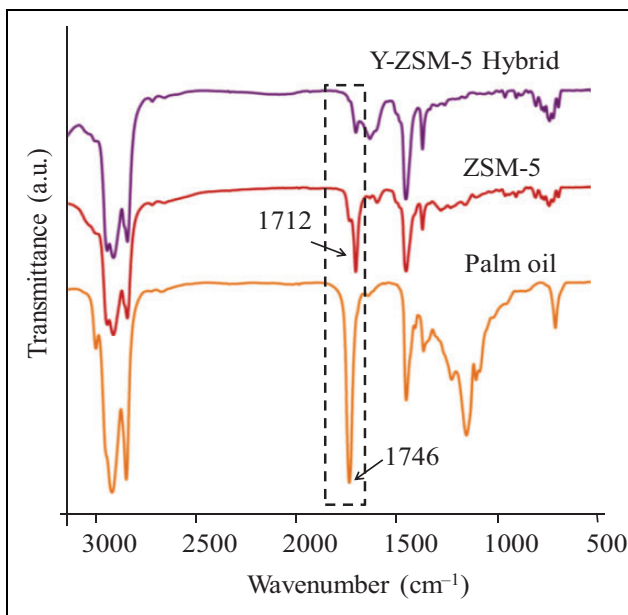
Figure 6. FTIR spectra of the palm oil and products generated using ZSM-5 and Y-ZSM-5 hybrid catalyst. FTIR: Fourier transform infrared.

Figure 7. Selectivity and liquid product distribution of hydrocarbons in jet biofuel. (a) Selectivity to alkane and aromatic hydrocarbons and (b) hydrocarbon distribution of jet biofuel converted from palm oil over zeolite catalysts.

very intense band at 1746 cm^{-1}, characteristic of the C=O stretch in esters that are predominantly found in palmist fats. After the reaction, there was a reduction of the band at 1712 cm^{-1}, which is attributed to the C=O stretch of carboxylic acids, the primary components of palmist fat hydrolysate.[31] Comparatively, an intense band at 1712 cm^{-1} was detected in jet biofuel over zeolite ZSM-5 catalyst, confirming the presence of carboxylic acids, as observed by the GC-MS. The intensity of the band decreased significantly when zeolite Y-ZSM-5 hybrid catalyst was used, suggesting that the deoxygenation process occurred with high efficiency. Nevertheless, palm oil was not fully converted into hydrocarbon compounds since the C=O band did not completely disappear after the reaction.

Typically, commercial jet fuel consists of three main components, including alkanes, cyclic alkanes, and aromatic hydrocarbons.[32] As shown in Figure 7(a), jet biofuel converted from palm oil contained a mixture of straight chain, iso- and cyclo-alkanes as well as aromatic hydrocarbons. Zeolite Y presented a high selectivity of *n*-alkane (51%) and the lowest selectivity of aromatic hydrocarbons (25%). Selectivity of jet biofuel alkane range and aromatic hydrocarbons over ZSM-5 catalyst is 56% and 26%, respectively. Although ZSM-5 shows high selectivity of *n*-alkane, the low yield of jet biofuel product makes this catalyst less efficient than zeolite Y.

In contrast, selectivity of *n*-alkane decreased to 45% over zeolite Y/ZSM-5 composite catalyst, while the selectivity of aromatic hydrocarbons was increased to 41%. Meanwhile, zeolite Y-ZSM-5 hybrid catalyst shows the lowest selectivity of *n*-alkane (30%), while the formation of aromatic hydrocarbons significantly increased to
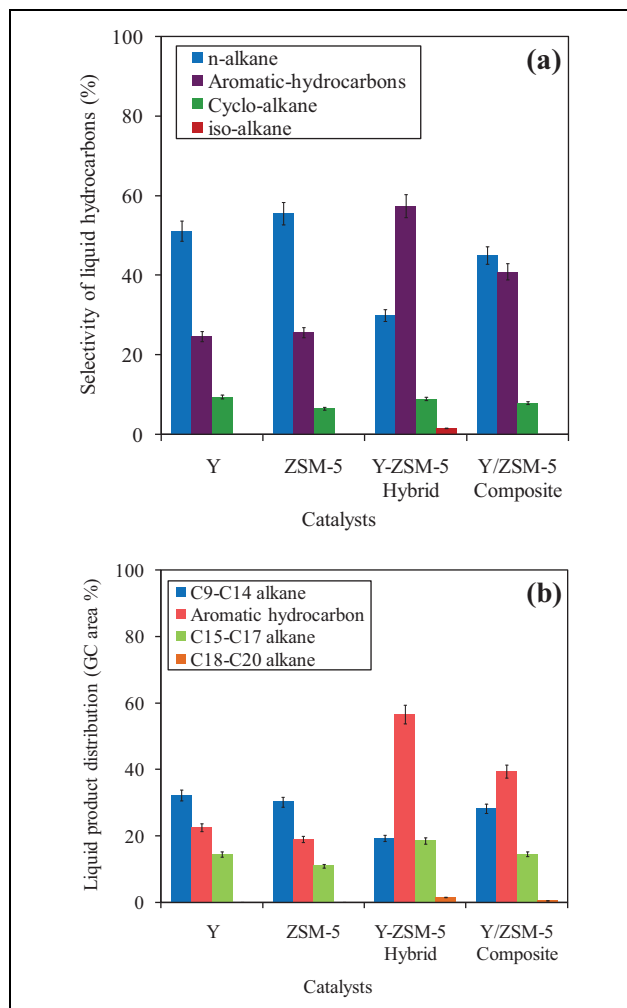
approximately 57%. This could be due to the contribution of two different pore structures. It is assumed that the use of zeolite Y as nutrients for the growth of ZSM-5 causes partial blockage of the largest pores. This suggests that large fatty acid molecules were deoxygenated into long-carbon chains in the cages or on the outer surface of zeolite Y and ZSM-5. Then, the long hydrocarbon chains were able to diffuse after being cracked into short-carbon chain alkanes (C14–C20) in the pore of zeolite Y. On the other hand, the reduced pore size of zeolite ZSM-5 due to partial blockage hampered the diffusion of the longer alkane unless they were further cracked into shorter carbon chains (C9–C13) and aromatic hydrocarbons. It should be reminded that an increasing number of aromatics would decrease the quality of jet biofuel.

Figure 7(b) depicts the distribution of C9–C20 alkanes and aromatics over different catalysts. Fatty acids in palm oil successfully decomposed into hydrocarbon of different
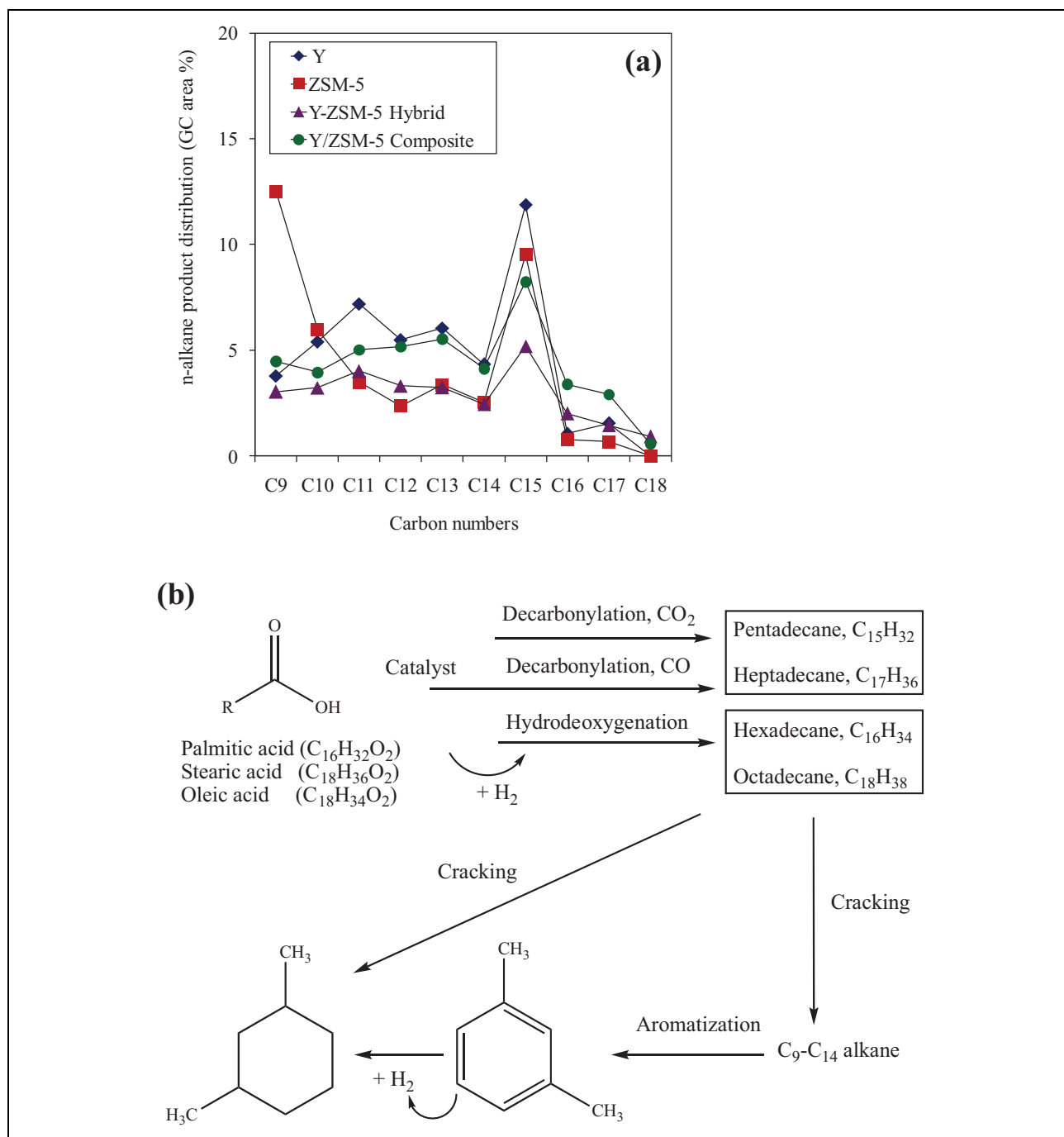
Figure 8. Comparison of the carbon number distribution of liquid product and reaction pathways from palm oil to jet biofuel: (a) *n*-alkane product distribution over zeolite catalysts and (b) reaction pathways of fatty acids in palm oil in the production of hydrocarbons.

alkane range. As shown in Figure 7(b), C9–C14 alkanes are the main products of hydrocarbon cracking over zeolite Y and ZSM-5 catalyst. Meanwhile, zeolites Y-ZSM-5 hybrid and Y/ZSM-5 composite catalysts resulted in the lowest and highest distribution of jet biofuel range alkane and aromatic hydrocarbons, respectively. Therefore, the result shows that catalytic conversion of palm oil to jet biofuel involves deoxygenation of fatty acids through decarbonylation or decarboxylation into high molecular straight-

chain alkanes (C15–C20), cracking into C9–C14 alkanes, and dehydrogenation into aromatic hydrocarbons through aromatization with H-transfer. The presence of C18–C20 alkanes over zeolite Y-ZSM-5 hybrid catalyst indicates that after deoxygenation, some of the hydrocarbons were not cracked into short-chain alkanes.

Figure 8(a) shows the product distribution of C9–C18 alkanes over different catalysts. These observations are the key points to propose the reaction pathway for the

conversion of fatty acid in palm oil into jet biofuels. Zeolites Y, Y-ZSM-5 hybrid, and Y/ZSM-5 composite produce a higher distribution of heavy chain alkanes (C11–C15) than zeolite ZSM-5. By contrast, zeolite ZSM-5 shows the highest distribution of light chain alkanes (C9) probably due to the smaller pore size leading to increased selectivity of light hydrocarbons. As shown in Figure 8(a), the heavy oxygen-free long-chain alkane needs to be cracked further into C9–C14 lighter alkanes to meet the strict jet fuel requirements.

The reaction pathway is proposed in Figure 8(b). The jet biofuel products from palm oil contain a considerable amount of odd carbon atoms (C13, C15, and C17), wherein the fatty acids only contain compounds with even number of carbons (C16 and C18). The alkanes with an odd number of carbons (heptadecane, pentadecane, and tridecane) are associated with decarboxylation and decarbonylation mechanisms, which produce alkanes with one less carbon than the original fatty acids. Nevertheless, hydrodeoxygenation process also occurred since hydrogen was supplied in the reaction resulted in a small amount of hexadecane (C16) and octadecane (C18), the same carbon atom of fatty acids. Then, the long-chain alkanes go through catalytic cracking in the presence of shape-selective zeolite catalysts to form alkanes in the range of nonane (C9) to dodecane (C12). The alkanes were further aromatized into aromatics with short-carbon chains, namely benzene, p/m-xylene, indane, and naphthalene. This study clearly shows that the jet biofuel (9–15 carbon atoms) consisting of straight-chain alkane, cyclic alkane, and aromatic hydrocarbon can be synthesized using palm oil in the presence of zeolites Y and ZSM-5 catalysts. However, further study is required to measure the recyclability of the above catalysts and prove its suitability for industrial applications.

Conclusions

In summary, a simple route was successfully developed for directly producing C9–C18 alkane, cyclo- and aromatic hydrocarbons from palm oil using heterogeneous zeolite catalysts in the presence of hydrogen in a fast pyrolysis process. A jet biofuel fraction from palm oil was enhanced over zeolite Y catalyst by increasing the distribution of jet range alkane and decreasing jet range aromatic hydrocarbon. The distribution of aromatic hydrocarbon range increased remarkably using zeolites Y-ZSM-5 hybrid (57%) and Y/ZSM-5 composite catalysts (41%). The highest conversion of palm oil to hydrocarbon compounds was achieved by zeolite Y-ZSM-5 hybrid catalyst (99%), followed by zeolite Y/ZSM-5 composite (96%), zeolite Y (91%), and zeolite ZSM-5 (74%). Zeolite Y-ZSM-5 hybrid is a suitable catalyst to convert all types of compounds in the palm oil to alkanes and aromatic hydrocarbons. Fatty acids in palm oil can be converted to liquid hydrocarbons by deoxygenation (decarboxylation, decarbonylation, and

hydrodeoxygenation), where decarboxylation and decarbonylation are the dominant reaction pathways, in addition to catalytic cracking and aromatization process. The recyclability of the samples should be measured to prove that the catalysts studied are suitable for industrial applications.

Declaration of conflicting interests

The author(s) declared no potential conflicts of interest with respect to the research, authorship, and/or publication of this article.

ORCID iD

Norsahika Mohd Basir https://orcid.org/0000-0001-9394-127X
Halimaton Hamdan https://orcid.org/0000-0001-9927-8448

References

1. Graham-Rowe D. Agriculture: beyond food versus fuel. *Nature* 2011; 474(7352): S6–S8.
2. Abdul K and Liwan A. Oil and gas trends and implications in Malaysia. *Energy Policy* 2012; 50: 262–271.
3. Rye L, Blakey S, and Wilson CW. Sustainability of supply or the planet: a review of potential drop-in alternative aviation fuels. *Energy Environ Sci* 2010; 3: 17–27.
4. Sawin JL, Seyboth K, and Sverrisson F. *Renewables 2016: global status report*. France: REN21-Renewable Policy Energy Network Secretariat, 2016.
5. Popp J, Lakner Z, Harangi-Rákos M, et al. The effect of bioenergy expansion: food, energy, and environment. *Renew Sustain Energy Rev* 2014; 32: 559–578.
6. Wang W-C and Tao L. Bio-jet fuel conversion technologies. *Renew Sustain Energy Rev* 2016; 53: 801–822.
7. Veriansyah B, Han JY, Kim SK, et al. Production of renewable diesel by hydroprocessing of soybean oil: effect of catalysts. *Fuel* 2012; 94: 578–585.
8. Duan J, Han J, Sun H, et al. Diesel-like hydrocarbons obtained by direct hydrodeoxygenation of sunflower oil over Pd/Al-SBA-15 catalysts. *Catal Comm* 2012; 17: 76–80.
9. Li T, Cheng J, Huang R, et al. Conversion pathways of palm oil into jet biofuel catalyzed by mesoporous zeolites. *RSC Adv* 2016; 6: 103965–103972.
10. Davis R, Aden A, and Pienkos PT. Techno-economic analysis of autotrophic microalgae for fuel production. *Appl Energy* 2011; 88: 3524–3531.
11. Klingshirn CD, DeWitt M, Striebich R, et al. Hydroprocessed renewable jet fuel evaluation, performance, and emissions in

a T63 turbine engine. *J Eng Gas Turbines Power* 2012; 134: 051506–051508.

12. Kumabe K, Sato T, Matsumoto K, et al. Production of hydrocarbons in Fischer-Tropsch synthesis with Fe-based catalyst: investigations of primary kerosene yield and carbon mass balance. *Fuel* 2010; 89: 2088–2095.

13. Griffin DW and Schultz MA. Fuel and chemical products from biomass syngas: a comparison of gas fermentation to thermochemical conversion routes. *Environ Prog Sustain Energy* 2012; 31: 219–224.

14. Gollakota ARK, Reddy M, Subramanyam MD, et al. A review on the upgradation techniques of pyrolysis oil. *Renew Sustain Energy Rev* 2016; 58: 1543–1568.

15. Bridgwater AV. Review of fast pyrolysis of biomass and product upgrading. *Biomass Bioenergy* 2012; 38: 68–94.

16. Abnisa F, Daud WMAW, Wan WMA, et al. Utilization possibilities of palm shell as a source of biomass energy in Malaysia by producing bio-oil in pyrolysis process. *Biomass Bioenergy* 2011; 35(5): 1863–1872.

17. Santillan-Jimenez E and Crocker M. Catalytic deoxygenation of fatty acids and their derivatives to hydrocarbon fuels via decarboxylation/decarbonylation. *J Chem Technol Biotechnol* 2012; 87: 1041–1050.

18. Diamantopoulos N. Comprehensive review on the biodiesel production using solid acid heterogeneous catalysts. *J Thermodyn Catal* 2015; 06(01): 1–8.

19. Hassani M, Najafpour GD, Mohammadi M, et al. Preparation characterization and application of zeolite-based catalyst for production of biodiesel from waste cooking oil. *J Sci Ind Res* 2014; 73(2): 129–133.

20. García-Martínez J, Johnson M, Valla J, et al. Mesostructured zeolite Y– high hydrothermal stability and superior FCC catalytic performance. *Catal Sci Technol* 2012; 2: 987–994.

21. Rahimi N and Karimzadeh R. Catalytic cracking of hydrocarbons over modified ZSM-5 zeolites to produce light olefins: a review. *Appl Catal A: General* 2011; 398: 1–17.

22. Hamdan H, Muhid MNB, Endud MS, et al. ^{29}Si MAS NMR, XRD and FESEM studies of rice husk silica for the synthesis of zeolites. *J Non Cryst Solids* 1997; 211(1–2): 126–131.

23. Hamdan H and Keat YA. *Synthesis of zeolite Y from rice husk ash*. Malaysia: Patent MY-115131-A, 1993.

24. Seo SM and Lim WT. Synthesis and single-crystal structures of fully dehydrated and highly proton-exchanged zeolites Y, $|H_{74}Na_1|[Si_{117}Al_{75}O_{384}]$-FAU and $|H_{73}Na_2|[Si_{117}Al_{75}O_{384}]$-FAU. *Bull Korean Chem Soc* 2009; 30(11): 2773–2776.

25. Mentzen BF. Crystallographic determination of the positions of the monovalent H, Li, Na, K, Rb, and Tl cations in fully dehydrated MFI type zeolites. *J Phys Chem C* 2007; 111(51): 18932–18941.

26. Majano G, Darwiche A, Mintova S, et al. Seed-induced crystallization of nanosized Na-ZSM-5 crystals. *Ind Eng Chem Res* 2009; 48: 7084–7091.

27. Pan M, Li P, Zheng J, et al. Zeolite-zeolite composite composed of Y zeolite and single-crystal like ZSM-5 zeolite: fabricated by a process like "Big fish swallowing little one". *Mater Chem Phys* 2017; 194: 49–54.

28. Huang S, Chen P, Yan B, et al. Modification of Y zeolite with alkaline treatment: textural properties and catalytic activity for diethyl carbonate synthesis. *Ind Eng Chem Res* 2013; 52: 6349−6356.

29. Shirazi L, Jamshidi E, and Ghasemi MR. The effect of Si/Al ratio of ZSM-5 zeolite on its morphology, acidity and crystal size. *Cryst Res Technol* 2008; 43(12): 1300–1306.

30. Cheng J, Li T, Huang R, et al. Optimizing catalysis conditions to decrease aromatic hydrocarbons and increase alkanes for improving jet biofuel quality. *Bioresource Technol* 2014; 158: 378–382.

31. Sousa FP, Cardoso CC, and Pasa VMD. Producing hydrocarbons for green diesel and jet fuel formulation from palm kernel fat over Pd/C. *Fuel Process Technol* 2016; 143: 35–42.

32. *Standard specification for jet turbine fuels*. West Conshohocken, PA: ASTM, 1994.